Proceedings of the ASME 2010 3rd Joint US-European Fluids Engineering Summer Meeting and
8th International Conference on Nanochannels, Microchannels, and Minichannels
FEDSM-ICNMM2010
August 1-5, 2010, Montreal, Canada

FEDSM-ICNMM2010-30406

STABILITY ANALYSIS OF CASSIE-BAXTER STATE UNDER PRESSURE DRIVEN FLOW

Tae Jin Kim
University of Texas at Austin
Austin, Texas, USA

Carlos H. Hidrovo
University of Texas at Austin
Austin, Texas, USA

ABSTRACT

The Cassie-Baxter state is a phenomenon in which a liquid rests on top of a textured surface with a gas layer trapped underneath the liquid layer. This gas layer introduces an effective shear free boundary that induces slip at the liquid-gas interface, allowing for friction reduction in liquid channel flows. Multiple studies have shown that different surface configurations result in different friction reduction characteristics, and most work is aimed at controlling the roughness factor and its shape in order to achieve an increased slip flow. This paper investigates the effects that different texturing geometries have on the stability of the Cassie state under pressurized microchannel flow conditions.

To test the stability effects associated with the pressurized microchannel flow conditions, microfluidic channels with microstructures on the side walls were designed and fabricated. The microstructures were designed to induce the Cassie state with a liquid-air interface forming between the texturing trenches. The air trapped within the microstructure is treated as an ideal gas, with the compressibility induced pressure rise acting as a restrictive force against the Wenzel wetting transition. The model was validated against experimental flow data obtained using microchannel samples with microtextured boundaries. The microchannels were fabricated in PDMS (poly-dimethylsiloxane) using soft lithography and were baked on a hot plate to ensure the hydrophobicity of the microtexture. Pressure versus flow rate data was obtained using a constant gravitational pressure head setup and a flow meter. The liquid-gas interface layer in the microchannel was visualized using bright field microscopy that allowed measurement of the liquid penetration depth into the microtexturing throughout the microhannel.

The experimental results indicate that air trapped in the pockets created by micro-cavity structures prevented the liquid layer from completely filling the void. As expected, the pressure drop in the micro-cavity textured channel showed a considerable decrease compared to that in the flat surfaced channel. These results also suggest that micro-cavities can maintain the Cassie state of a liquid meniscus, resting on top of the surface, in larger pressure ranges than open spaced micro-pillars arrays.

INTRODUCTION

Superhydrophobicity has recently received attention as a means of achieving surface friction and drag reduction [1]. Other applications include frost prevention on aircraft flight surfaces to self-cleaning features on solar energy panels [2].

Superhydrophobicity can be achieved by modifying the surface geometry. Two models represent the wetting behavior of the textured surface: the Wenzel state [3] and the Cassie-Baxter state [4]. The Wenzel state models the amplifying effect that surface texturing has on the Young's contact angle under fully liquid imbibed conditions. The Cassie-Baxter state models the macroscopic contact angle formed when air pockets exist within the microtexturing. The presence of these air pockets in the Cassie state can lead to friction and drag reduction [5], with research is this area being actively pursued. Such research includes modeling the fluid flow over random textured surfaces [6], studying the drag reduction of flow over carbon nano-tube forests [7], and the use of chemical coatings in microtextured surfaces to induce superhydrophobic conditions [8], among others.

Despite the vast literature on friction and drag reduction from superhydrophobic surfaces there is very little work aimed at understanding the, pressure effects on the stability and characteristics of this condition. A few researchers have studied the pressure effects on the Cassie-Baxter State, concluding that textured surfaces with isolated gaps result in a lower contact angle hysteresis [9]. However, experimental studies on the compressibility effects from the trapped gas layer have not been conducted to date. Our aim is to study the pressure effects associated with this compression in order to elucidate how they affect the stability of the Cassie state and its friction reduction characteristics.

In this paper, we develop a simple model of the compressibility effects associated with the gas pockets and the corresponding modifications introduced by it into the Cassie-Baxter equation.

This model is validated against experimental microchannel flow data, where micro-gaps are used as the surface texturing. The flowing fluid in the microchannels tends to penetrate into the micro-cavity gaps as a result of the imposed pressure gradient. Consequently, the pressure of the gas increases as the fluid pushes into the cavity, preventing the fluid from completely wetting it. Correlation of the model results and experimental data indicates that shallower cavities provide more stability to the Cassie state under pressure flow conditions, despite falling below the theoretical critical roughness value.

NOMENCLATURE

γ_{LV}	Surface tension in the liquid-vapor interface
μ	Dynamic viscosity of water
θ_{C-B}	Cassie-Baxter angle
θ_Y	Young's contact angle
ϕ_s	Solid contact area ratio
P_l	Liquid pressure
P_{atm}	Atmospheric pressure
ΔP	Pressure drop
Q	Flow rate
r_c	Critical roughness
y	Penetration depth
Y	Depth of cavity
p	Perimeter of cavity
A_c	Cross-sectional area of the cavity
h	Height of the microfluidic channel
w	Width of the microfluidic channel
L	Length of microfluidic channel

THEORETICAL MODEL

Cassie-Baxter Model

In order to ensure proper drag/friction reduction in the microchannels flows, a microtextured surface that induces a stable Cassie state is desirable. A liquid meniscus, resting on top of a textured surface, is under a Cassie state if it does not wet the gaps beneath the liquid interface. With an air layer underneath the contact surface, the liquid droplet experiences less friction. In addition, the liquid resting on top of the textured surface will experience a decrease in surface resistance since a portion of the contact surface underneath is gas. The standard Cassie-Baxter model [4] is,

$$\cos\theta_{C-B} = \phi_s \cos\theta_Y - (1-\phi_s) \qquad (1)$$

where θ_{CB} is the Cassie-Baxter angle, θ_Y is the Young's contact angle, and ϕ is the ratio of solid contact area to the nominal area.

To ensure the Cassie state, the surface topography must be rougher than the critical roughness factor[10],

$$r_c = \phi_s - \frac{1-\phi_s}{\cos\theta_Y} \qquad (2)$$

where r_c is the critical roughness factor. A roughness factor lower than r_c will result in a Wenzel state where full wetting of the microtextured surface will occur, or a metastable Cassie state where the liquid initially under Cassie state may transition to Wenzel state if disturbances occur. On the other hand, a roughness factor higher than r_c will lead to a stable Cassie state. In our experiment, we have explored textured microfluidic channels with roughness factors higher and lower than the critical roughness factor.

Compression Effects on the Cassie-Baxter Model

The traditional Cassie-Baxter model assumes a zero pressure gradient, and the shape of the liquid interface is assumed to be flat [4]. In internal flows, however, the flow is driven by a pressure gradient. This longitudinal pressure gradient also affects the normal direction, imposing a varying pressure to the microtextured surface. If the microtextured geometry forms closed cavities, a series of isolated air pockets will be created. The liquid-gas interface formed by these air pockets will hold until the pressure in the microfluidic channel exceeds the surface tension holding the liquid-gas interface; penetration of the liquid layer into the air pockets will occur, thus compressing the air pockets. This compression leads to a pressure increase in the cavity that resists the penetration. Thus, in the pressure driven flow, the liquid-air interface equilibrium location is determined by the coupling of the surface tension and the compressibility effects in the air pockets.

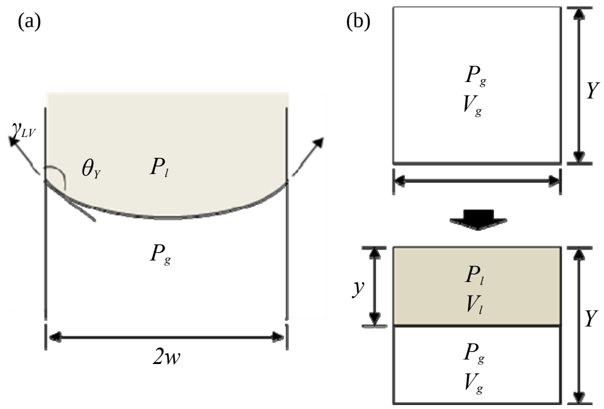

Fig. 1 (a) Schematic representation of capillary pressure being affected as liquid penetrates into the air pocket. (b) Surface curvature is simplified to a flat shape in order to estimate the penetration depth.

Modeling of the compressibility effects require a few assumptions: 1) the gas is considered to be ideal, 2) the temperature of the water and air is assumed to be at 25ºC and 3) the properties of the surface are assumed to be that of a cured PDMS with a static contact angle of 105º. Initially, the liquid will flow over the cavities, forming a liquid-gas interface in the cavities. However, if the applied pressure exceeds the resisting surface tension, the liquid portion will invade the cavities. The gas will start to compress and experience an increase in resisting pressure. By substituting in the ideal gas model into the Laplace pressure equation, the penetration depth can be estimated as,

$$y = Y\frac{P_l - P_{atm} - \dfrac{p}{A_c}\gamma_{LV}\cos(\pi-\theta_Y)}{P_l - \dfrac{p}{A_c}\gamma_{LV}\cos(\pi-\theta_Y)} \qquad (3)$$

where y is the penetrated depth into the cavities, P_l is the liquid pressure, Y is the depth of the cavity, and γ_{LV} is the surface tension at the liquid-vapor interface.

EXPERIMENTAL SETUP

Fabrication of the Micro-cavity Substrate Microchannels

The microfluidic device was fabricated by soft-lithography. A bare wafer was coated with Su-8 2050 (Microchem) and a negative mold for the PDMS microfluidic channel was fabricated through standard photolithographic procedures. The thickness of the Su-8 mold pattern was measured using a profilometer (Veeco) to confirm the channel thickness.

The wafer was then silanized (UCT specialties, LLC) for at least an hour in a vacuum desiccator to fluorinate the Su-8 mold. A PDMS base and solvent (Dow Corning) mixture, mixed at a volume ratio of 9:1, was poured on the silanized Su-8 mold. The entire wafer was cured at 95°C for 2 hours.

The cured PDMS microfluidic channel replicas were peeled off from the wafer and were bonded to glass substrates. Prior to bonding, the glass substrates were spin coated with a thin layer of PDMS to ensure uniform properties within the microfluidic channel. Both PDMS slabs and PDMS coated glass substrates were treated with oxygen plasma (Harrick Plasma) at 29Watts for 20 seconds. Once the bonding was complete, the treated samples were then baked overnight on a hot plate at 95°C.

The channel dimensions for the baseline channel with no surface textures are 60µm × 60µm × 2cm (width × height × length). For the channels with micro-textured surface, there are four different configurations in the cavity dimensions: 30µm × 30um (gap size × depth of cavity), 30µm × 15mm, 60µm × 30um and 60µm × 15mm.

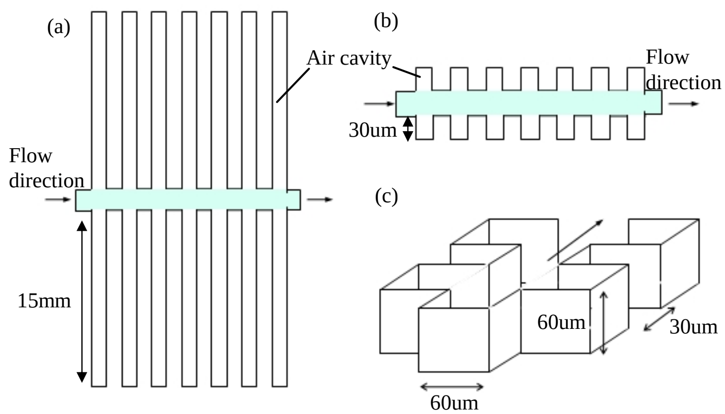

Fig. 2 Schematic diagrams of (a) 30µm spacing with deep trenches, (b) 30µm spacing with shallow trenches, and (c) a 3-d view of 30µm spacing with shallow with shallow trenches.

Constant Pressure Source

A water reservoir with variable liquid column height was used to generate a constant pressure source. The outlet of the water column device was connected to the microchannels. By controlling the height of the water column, a constant pressure conditions ranging from 600Pa to 6600Pa were able to be applied to the microfludic channel. The flow rate corresponding to the pressure was measured using a high-precision scale.

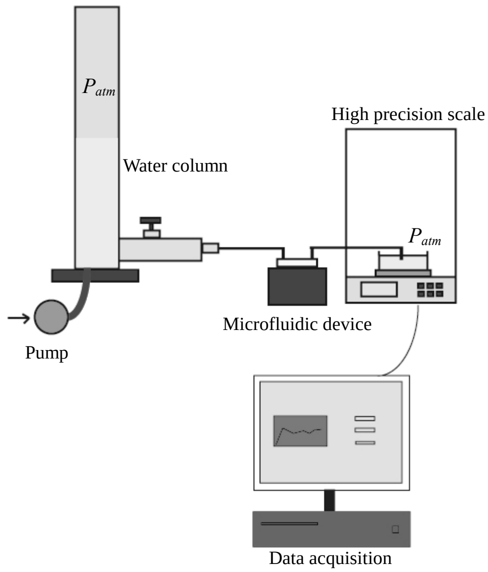

Fig. 3 Experimental setup of pressure measurement test

RESULT

Pressure Effects on Penetration Depth

The pressure driven flow in the microfluidic channel was generated by the constant pressure source. With a constant pressure applied to the microfluidic channel, the pressure is ρgh at the inlet and atmospheric pressure at the outlet. Depending on the constant pressure source, this pressure gradient will either wet the cavity or maintain the Cassie State. Since the connecting tubes are large compared to the microfluidic channel, the head losses due to these tubes are negligible.

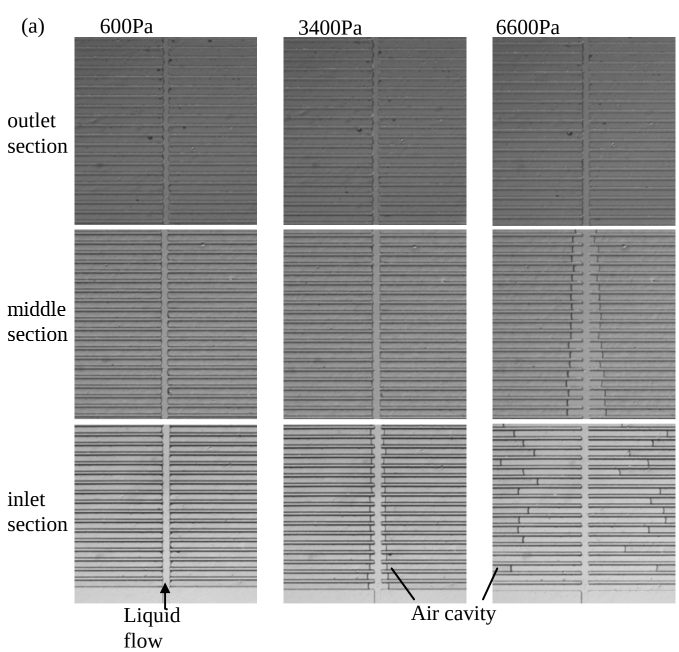

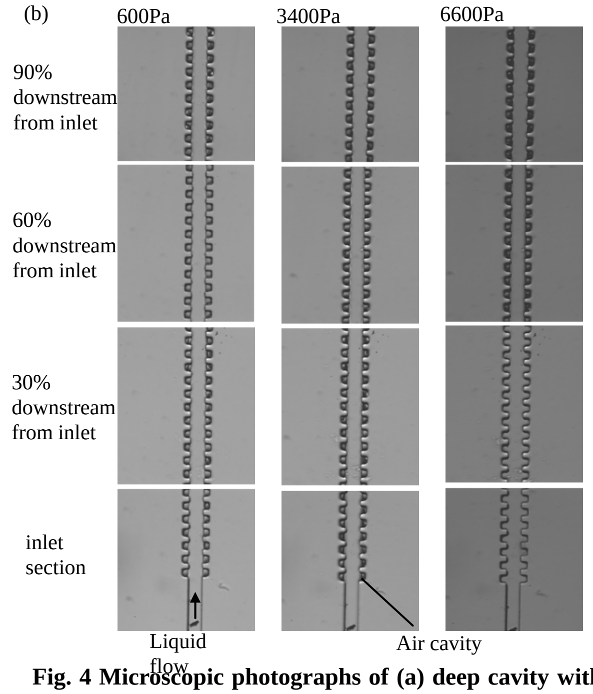

Fig. 4 Microscopic photographs of (a) deep cavity with 60µm gap size (4x) and (b) shallow cavity with 30µm gap size (10x). Liquid layer is surrounded by air pockets formed in the trenches.

The images in Figure 4 visually depict the relationship between pressure and penetration depth in the cavities, where the penetration depth is measured using a micro-scale. The pressure is the largest near the inlet and the smallest near the outlet. When the inlet pressure is large enough to overcome surface tension penetration within the cavity was observed.

In the figure, two channel configurations were used to induce resisting gas phase pressures: one with shallow cavities with a depth of 30 µm, and the other with deep cavities with a depth of 15 mm. For the channel with deep cavities, 50% of the cavities showed penetration at 3400Pa for the channels with a gap size of 30µm and at 3000Pa for the channels with a gap size of 60µm. For the channel with shallow cavities, 50% of the cavities showed penetration at 4200Pa for the channels with a gap size of 30µm and at 3800Pa for the channels with a gap size of 60µm. For the channel with shallow cavities, penetration generally occurred at higher pressures but at random locations. Figure 4(b) shows that the filling of the gaps can be delayed if the gaps are isolated, and air can be compressed to resist penetration.

From the above results, it can be seen that the air trapped inside the microcavities act as a penetration resistance mechanism that can maintain the Cassie state. The higher the pressure, the more the air within the cavity will be compressed, and henceforth the higher the resistance against penetration.

Friction Reduction Effects

The baseline of the experiment is the channel with no cavities. The dimensions of the channel are 60μm × 60μm × 2cm (width × height × length). For a square duct the flow rate is given by [11],

$$Q = \frac{hw^3}{12\mu}\left(\frac{\Delta P}{L}\right)\left[1 - \frac{192w}{\pi^5 h}\sum_{i=1,3,5...}^{\infty}\frac{\tanh\left(\frac{i\pi h}{2w}\right)}{i^5}\right] \quad (4)$$

where h is the height of the channel, w is the width of the channel, L is the length of the channel, ΔP is the pressure difference in the channel and Q is the flow rate.

From figure 5, the experimental data agrees well with the theoretical model. Based on this data, we can assume that the experimental results will be reliable for channels with cavities as well.

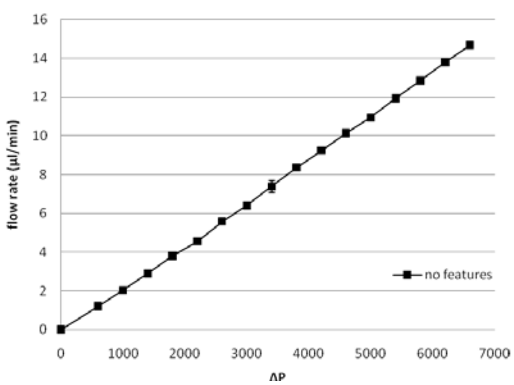

Fig. 5 Flow rate vs. ΔP graph for channel with no features

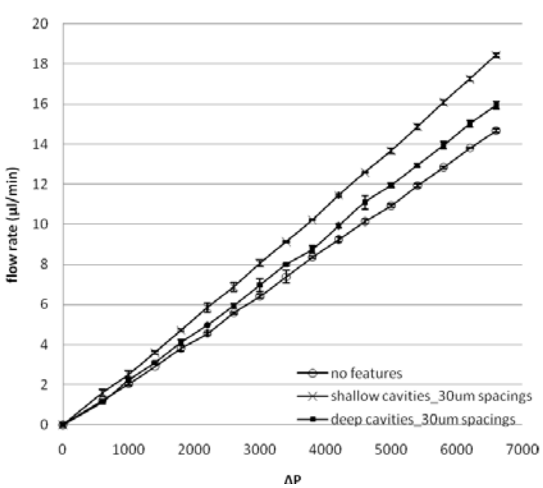

Fig. 6 Flow rate vs. ΔP graph for 30μm cavity channels

Figure 6 represents the flow rate vs. ΔP for the channel with 30μm gaps between the micro-textures. For both the shallow and the deep cavities cases, the data showed good repeatability with a small standard deviation from the average value. However, it is evident that the shallow cavity channel had the highest flow rate among the three cases, with the deep cavity channel following the second. This is anticipated since the liquid-gas interface in the shallow cavity channel is maintained at higher pressures than the deep cavity channel. However, the flow rate is likely to be influenced by the extra friction induced by the wetted walls where the liquid has penetrated into the cavities.

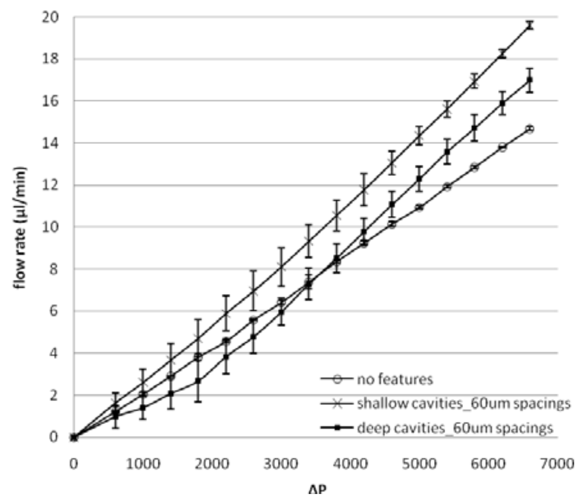

Fig. 7 Flow rate vs. ΔP graph for 60μm cavity channels

Unlike the previous case, the results for the channel with 60μm gaps between the micro-textures were less consistent, as can be seen in figure 7. For both shallow and deep cavity case, the data is dispersed and the slope of the graph is less linear than the 30μm gap channel. This behavior may have occurred due to the larger gap size of the cavities, where the liquid-gas interface gets disrupted at lower pressures. Particularly for the shallow cavity case, there were instances where the flow rate was the highest among all the channel configurations. This may be accredited to random fillings of the cavities during the channel priming stage.

CONCLUSION

In this paper we investigated the effect that trapped air has on the stability of the Cassie state for friction reduction purposes in pressure driven microchannel flow. The side walls of the PDMS microchannels were grooved to form air pockets in the liquid channel flow.

A constant pressure source was used to flow water into the microfluidic channel and the flow rate was measured using a high-precision scale. It was found that the flow rate for microchannels with shallow microcavities on the side walls were greater than that of the channels with deep cavities. We also observed that the flow rate was the highest in the 60µm gap shallow channel. However, the Cassie State for these samples was relatively more unstable as compared to the 30µm gap shallow channels, and liquid penetration into the air pockets occurred at lower pressures. In general, however, the channels with shallow microcavities withstood higher pressure ranges than the channels with deep microcavities.

It was also found that micro-cavities can maintain the Cassie state in larger pressure ranges than open space gap geometries, such as micropillar arrays. This is the result of a penetration resistance effect arising from compressibility of the entrapped air.

These results indicate that higher roughness might not necessarily correlate to a more stable Cassie state, and that surfaces with isolated air pockets may actually be more stable than a surface that is non-isolated but with a higher roughness factor. Hence, we anticipate that the effect of air pockets can be extended to the designing of superhydrophobic surfaces exposed to external fluid flow.

REFERENCES

[1] Ma, M., and Hill, R. M., 2006, "Superhydrophobic Surfaces," Current Opinion in Colloid & Interface Science, 11(4), pp. 193-202.

[2] Furstner, R. and Barthlott, 2005, "Wetting and Self-Cleaning Properties of Artificial Superhydrophobic Surfaces," Langmuir, 21, pp. 956-961.

[3] Wenzel, R. N., 1936, "Resistance of Solid Surfaces to Wetting by Water," Industrial & Engineering Chemistry, 28(8), pp. 988-994.

[4] Cassie, A. B. D., and Baxter, S., 1944, "Wettability of Porous Surfaces," Transactions of the Faraday Society, 40(pp. 546-551.

[5] Choi, C. H., Ulmanella, U., Kim, J., Ho, C. M., and Kim, C. J., 2006, "Effective Slip and Friction Reduction in Nanograted Superhydrophobic Microchannels," Physics of fluids, 18, pp. 087105.

[6] Gogte, S., Vorobieff, P., Truesdell, R., Mammoli, A., Van Swol, F., Shah, P., and Brinker, C. J., 2005, "Effective Slip on Textured Superhydrophobic Surfaces," Physics of fluids, 17, pp. 051701.

[7] Joseph, P., Cottin-Bizonne, C., Benoit, J. M., Ybert, C., Journet, C., Tabeling, P., and Bocquet, L., 2006, "Slippage of Water Past Superhydrophobic Carbon Nanotube Forests in Microchannels," Physical review letters, 97(15), pp. 156104.

[8] Ou, J., Perot, B., and Rothstein, J. P., 2004, "Laminar Drag Reduction in Microchannels Using Ultrahydrophobic Surfaces," Physics of fluids, 16, pp. 4635-4643.

[9] Bahadur, V., and Garimella, S. V., 2008, "Electrowetting-Based Control of Droplet Transition and Morphology on Artificially Microstructured Surfaces," Langmuir, 24(15), pp. 8338-8345.

[10] Lafuma, A., and Quere, D., 2003, "Superhydrophobic States," Nature materials, 2(7), pp. 457-460.

[11] White, F. M., 2006, <u>Viscous Fluid Flow</u>, Mcgraw-Hill, 3rd ed., pp. 113.